Nanotechnology **19** (2008) 095504 (5pp) doi:10.1088/0957-4484/19/9/095504

Nanopillar arrays on semiconductor membranes as electron emission amplifiers

Hua Qin[1], **Hyun-Seok Kim and Robert H Blick**

Department of Electrical and Computer Engineering, University of Wisconsin-Madison, 1415 Engineering Drive, Madison, WI 53706, USA

E-mail: QIN1@WISC.EDU and hqin2007@sinano.ac.cn

Received 5 October 2007
Published 11 February 2008
Online at stacks.iop.org/Nano/19/095504

Abstract

A new transmission-type electron multiplier was fabricated from silicon-on-insulator (SOI) material by integrating an array of one-dimensional (1D) silicon nanopillars onto a two-dimensional (2D) silicon membrane. Primary electrons are injected into the nanopillar–membrane (NPM) system from the flat surface of the membrane, while electron emission from the nanopillars is probed by an anode. The secondary electron yield (SEY) from the nanopillars in the current device is found to be about 1.8 times that of the plain silicon membrane. This gain in electron number is slightly enhanced by the electric field applied from the anode. Further optimization of the dimensions of the NPM and an application of field emission promise an even higher gain for detector applications and allow for probing of electronic/mechanical excitations in an NPM system stimulated by incident particles or radiation.

(Some figures in this article are in colour only in the electronic version)

1. Introduction

The interaction of energetic particles with matter is a fundamental process in physics. Many interaction pathways exist, leading to the production of a variety of secondary particles. Arguably the most important of these processes is the so-called secondary electron emission (SEE), which in addition to its importance in material properties also serves as the basis for a broad variety of widely used practical devices (e.g. electron multipliers, cathode ray screens, and silicon detectors) [1–8]. In the case of SEE stimulated by primary electrons (PEs), the secondary electron yield (SEY) is determined by the balance between two opposing effects. On the one hand, the thicker the layer of material interacting with the primary particles, the greater the probability of an electron-generating event. However, at the same time, as the penetration depth of primary electrons increases, the ability of a secondary electron (SE) to escape from the material decreases. This determines that SEE is an effect that mainly occurs near the surface, and a grazing incident angle produces more SEs [1, 9]. It has been found that a proper surface roughness can enhance SEE, while large corrugations suppress SEE. Recently, it has also been found that SEE can be either enhanced or suppressed by carbon nanofibers, depending on whether the nanofibers are suspended from or attached to the underlying silicon substrate [10]. Unlike this random configuration of carbon nanofibers or conventional surface roughness produced in a sputtering process for metallic/dielectric material deposition, the advances in nanofabrication and material science now allow for precise engineering of surfaces to optimize SEE and understanding new physics of electron impact on nanoobjects. Here we demonstrate a nanostructured material consisting of an array of one-dimensional (1D) silicon nanopillars fabricated on the surface of a suspended two-dimensional (2D) layer of crystalline silicon. It is shown that this juxtaposition of structures of different dimensionalities results in an enhanced SEE response. The choice of a thin membrane allows for a separation of primary and secondary electrons, i.e., a transmission-type electron generation. Naturally, this scheme is easy to extend to other materials with excellent electron emission properties, such as diamond nanopillars, aligned carbon nanotubes and zinc oxide nanowires. This ability to alter material properties by manipulation of device geometry at the nanoscale level opens new opportunities for exploring

[1] Present address: Suzhou Institute of Nano-Tech and Nano-Bionics, Chinese Academy of Science, 150 Renai Road, Suzhou City, Jiangsu 215123, People's Republic of China.

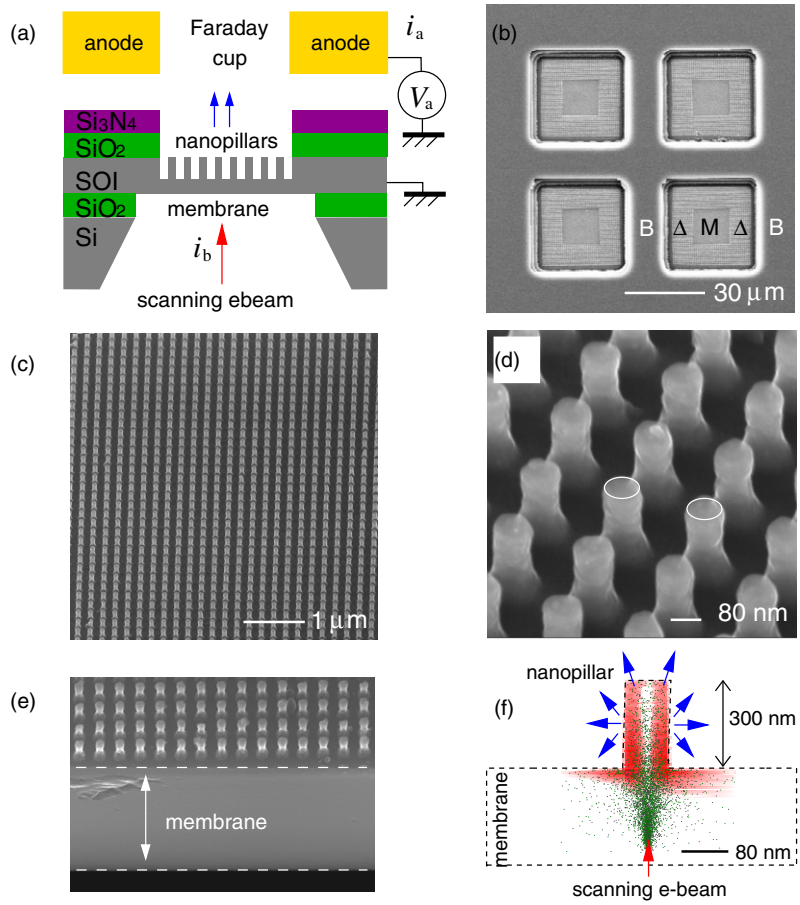

Figure 1. (a) Schematics of the NPM device and the experimental setup; (b), (c), (d), and (e) are scanning electron micrographs. (b) A top view of four square membranes; (c) and (d) are close views of a nanopillar array. (e) A cross section of the membrane. (f) A Monte Carlo simulation shows the different distributions of PEs (dots, color online) penetrating from beneath and SEs (gray scale, red online) in an NPM structure (see text for details).

electronic and mechanical excitations in nanostructures and new designs of novel materials and devices.

2. Experiment

For the purpose of this experiment we fabricated several NPM devices from silicon-on-insulator (SOI) wafers, as schematically shown in figure 1(a). Both the SOI and the silicon substrate have a crystal orientation of (100) and are n-type with a resistivity of 12 Ω cm. The SOI was thinned by thermal oxidation and capped with a thin layer of silicon nitride. On each NPM device, 16 square silicon membranes with a thickness of ≈1.6 μm and a side length of 35 μm were patterned into four 2 × 2 arrays. A scanning electron micrograph of four such membranes is shown in figure 1(b). On each membrane, an array (≈17 600) of round nanopillars was fabricated from the membrane host by electron-beam lithography and reactive-ion etching. Each pillar has a diameter of 80 nm and a height of 300 nm. Close-ups of nanopillar arrays with a pitch of 200 nm are shown in figures 1(c) and (d). In figure 1(e), the scanning electron microscope (SEM) image of a cleaved membrane reveals the overall architecture of 1D nanopillars placed on a 2D membrane. Also indicated in figure 1(b) is that the nanopillars are patterned in a frame marked by Δ around the center piece of the plain membrane marked by M. This allows one to discriminate electron transmission through the membrane alone (M), the NPM system (Δ), and through the bulk material (B) which includes two extra layers of dielectrics.

The experimental setup we used is also shown schematically in figure 1(a): the device is mounted in a scanning electron microscope (SEM) which provides a vacuum environment ($p \sim 10^{-6}$ mbar) and most importantly a controllable electron beam (e-beam). The e-beam is scanned over the backside of the membrane to inject electrons in the energy range of E_p = 1–30 keV. A Faraday-type anode is placed above the nanopillars, providing an extraction or retarding voltage for electrons emitted from the NPM device. By controlling the anode voltage (V_a) while monitoring the anode current (I_a), secondary electron emission ($E \lesssim 50$ eV) can be differentiated from electrons transmitted through the membrane (50 eV $< E \leqslant E_p$) [1] or from field emitted electrons[2]. This provides a simple method to analyze the energy distribution of emitted electrons and allows for identifying the effect of the nanopillars on electron emission. This experimental setup is similar to a scanning transmission electron micro-

[2] The total energy of field emitted electrons depends on the anode voltage applied.

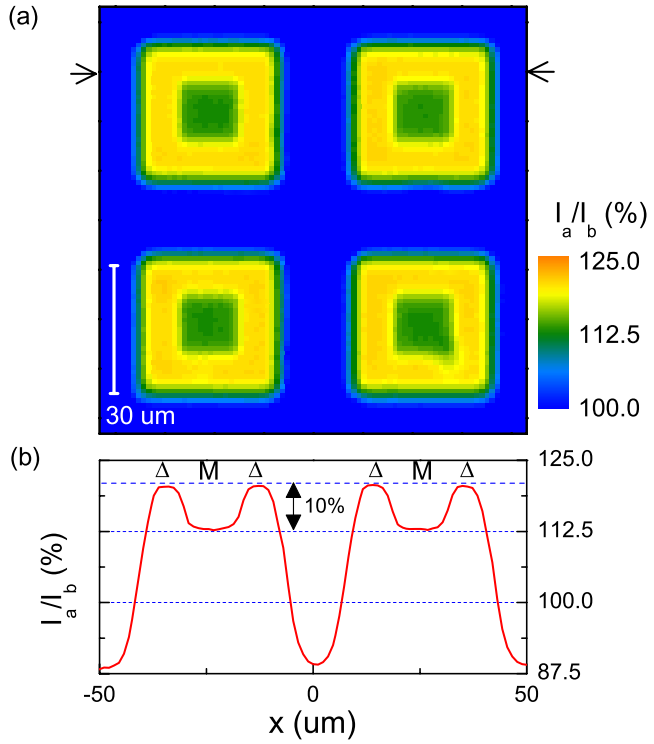

Figure 2. (a) A color-scale plot of the anode current as a function of the position of the scanning e-beam ($V_a = +200$ V, $E_p = 30$ keV, $I_b = 200$ pA). (b) A line scan taken between the two arrows shown in (a).

scope (STEM) [11, 12]. However, our experimental results demonstrate that electron emission is enhanced by introducing nanopillars on the emission surface of a thin membrane.

Figure 1(f) shows a Monte Carlo simulation revealing the spatial distribution of PEs (dots, color online) entering from below and the SEE (gray scale, red online) being emitted from the top surface in an NPM device. In the simulation, the real dimensions were used for the nanopillar. The membrane thickness was chosen to be same as the height of the nanopillar to reduce the simulation time. The electron energy was set at 30 keV. As will be shown below, in our nano-engineered NPM device, it is precisely the electron–solid interaction *within the nanopillars* that enhances the overall electron generation. In other words, the surface increase by 1D nanopillars enhances SEE to a degree where the membrane amplifies the incoming number of electrons more effectively than a 3D system. Thus adding the dimensions 2D + 1D as for the NPM system leads to a behavior different from that of a 3D bulk system.

3. Results and discussion

Figure 2(a) shows a color-scale map of the anode current (normalized by the incident beam current I_b) obtained from a raster scan of the e-beam. This map can be compared directly with the SEM image shown in figure 1(b). We find that the anode signal provides a high contrast in membrane thickness and most importantly shows a clear enhancement of electron emission in the area Δ. The plot in figure 2(b) represents a line scan taken from the corresponding color-scale map. Obviously, one can directly follow transitions between the non-membrane area (B), membrane (M) and membrane with nanopillars (Δ). The origin of this enhancement is identified as SEE from the nanopillars. Since an anode with a negative potential will keep electrons with energy below $e|V_a|$ from reaching the anode, it thus provides a method to analyze the energy of emitted electrons. The I_a–V_a characteristics in figure 3(a) were taken for three distinct areas (B, M and Δ) for comparison. Constant levels of anode current are observed when $V_a < -150$ V. These levels reflect the contribution from those electrons transmitted through the NPM system where the electrons' energy is only slightly attenuated ($E \leqslant E_p =$

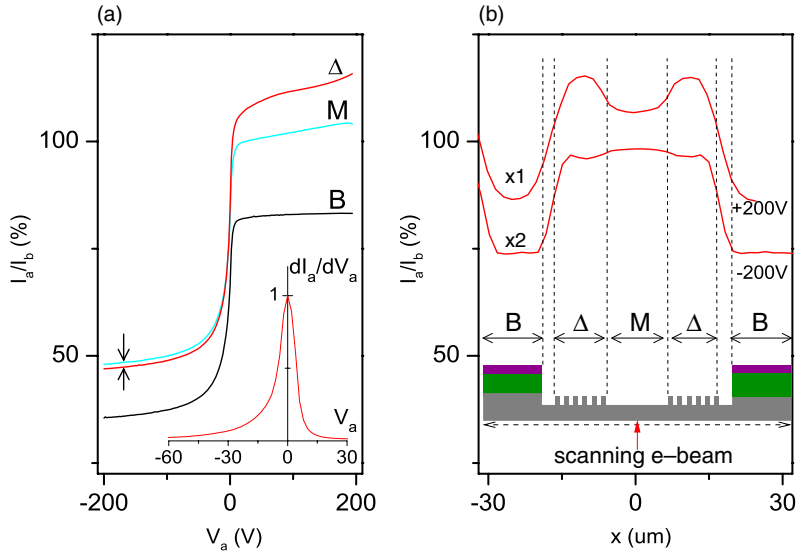

Figure 3. (a) The I_a–V_a characteristics were measured for comparison when the e-beam was located in areas B, M and Δ. The inset displays the energy distribution of SEs emitted from area Δ. (b) Two line scans across a single membrane were taken at $V_a = -200$ and $+200$ V for comparison. For clarity, the line scan taken at $V_a = -200$ V is multiplied by a factor of 2 ($E_p = 30$ keV, $I_b = 200$ pA).

30 keV). Upon further increasing the anode voltage up to +30 V, a continuous rise in the anode current due to SEE is found. Above $V_a = +30$ V, most transmitted PEs and SEs are collected by the anode and the anode current reaches a saturation value. In figure 3(a), the black curve shows the electron emission through the non-membrane area (B), which is suppressed in reverse bias to 36% and increased in the forward direction to about 83%. The increase of 47% is the contribution from SEs. Turning now to the signals from the membrane (M) and the NPM system (Δ), we can see that the direct transmission of PEs is increased by about 12% due to the thinness of the membrane compared to area B. However, the contribution from SEE is increased to 57% for area M and 67% for area Δ. Because of the increase in SEE, the total emission current becomes greater than the incident current, i.e., a gain is achieved. As depicted in the inset of figure 3(a), the derivative of the Δ-trace with respect to the anode voltage represents the energy distribution of the SEs, which is identical to that of area M.

We found that in contrast to the intuitive assumption—that is the thinner the membrane the higher the transmission should be—a membrane with nanopillars shows an even more enhanced signal. We further examined the effects of nanopillars on electron emission by scanning the e-beam (30 keV) across the nanopillar frame at $V_a = \pm 200$ V. Electron emissions from areas B, M and Δ are again compared directly in figure 3(b), where a remarkable influence of the nanopillars (Δ-peaks) is seen. Under a forward anode bias $V_a = +200$ V, the same as that in figure 2(b), an enhancement of SEE by the nanopillars is clearly observed. Under reverse anode bias $V_a = -200$ V, transmission of PEs is slightly *suppressed* by the nanopillars, which is also seen in figure 3(a) (see the arrows). This is a clear indication that the nanopillars absorb high-energy PEs and generate more low-energy SEs than the 2D membrane alone.

The above results were obtained for the incident energy of $E_p = 30$ keV. The detailed dependence of SEY on E_p is shown in figure 4. Again emission signals from area M and Δ are compared for $V_a = +200$ V. The threshold energy for electrons to 'penetrate' the NPM system is about 12.5 keV. There is no observable shift in the threshold energy comparing areas M and Δ. However, nanopillars significantly increase the emission signal—that is the yield $\gamma = \gamma(\gamma_m, \gamma_p)$, where γ_m and γ_p are the yields of SEE for membrane and nanopillars, respectively[3]. The solid line shown in figure 4 is a Monte Carlo approximation to the SEE from plain membranes, based on the Bethe model of energy loss and a parametric model of SEE [1, 13, 14]. Above the threshold energy of 12.5 keV, an enhancement of 180% by the nanopillars is obtained as compared to the membrane. Above 30 keV, which is the maximal energy available in our SEM, a saturation of the anode current levels is expected. The cause for this enhancement is obviously the altered surface morphology due to the nanopillars, which increases the effective surface area and the effective incident angle for electrons (see the Monte Carlo simulation in figure 1(f)). In the frame of this interpretation, the normalized anode current, defined as the total yield $\gamma = I_a/I_b$, can be expressed as $\gamma = \beta\gamma_p + (1-\beta)\gamma_m$, where β is the coverage of the membrane surface by nanopillars. For the area Δ on this particular device, we have $\beta = \pi d^2/4L^2 \approx 0.13$, where d is the diameter of a nanopillar, and L is the pitch distance. Consequently, a higher SEE can be achieved by decreasing the pitch distance between nanopillars: by reducing the pitch distance from 200 to 150 nm, while maintaining the pillar's dimension, β can be doubled. In the current device, the thickness of the membrane is much larger than the mean free path of the incident electrons, meaning that a large number of PEs are slowed down by scattering before they enter the nanopillars. Longer nanopillars will substantially increase both the generation and emission of SEs. A larger diameter for the nanopillars increases the emission area; however, it also reduces the possibility for secondary electrons to escape from the nanopillars. Hence, there is an optimized diameter corresponding to the energy of incident electrons.

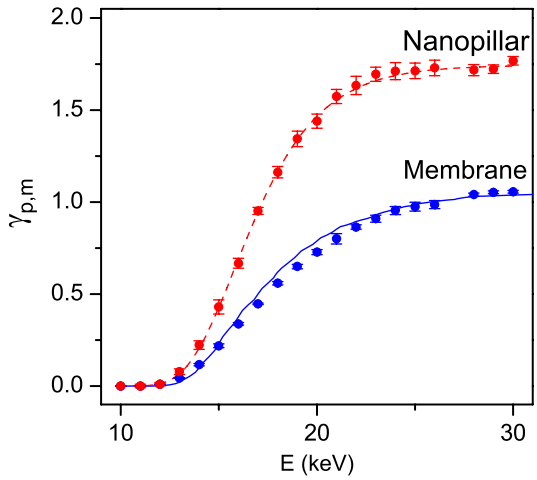

Figure 4. The dependence of SEY on the incident electron energy is compared for areas M and Δ. The solid line is a Monte Carlo simulation for area M ($V_a = +200$ V).

Compared to curve B in figure 3(a), it has to be noted that curve M has a stronger dependence on the positive anode potential. This is directly related to the fact that the electric field in the recessed membrane area is retarded (see figure 1(a)). The even stronger dependence on the anode potential found in area Δ stems from the suppression of the electric field on the nanopillar's sidewall by neighboring nanopillars. This suggests that the SEE from a patterned/rough surface could be maximized by an electric field applied so that the reentrance of SEs into neighboring nanopillars is avoided. A factor of 10 in the enhancement of SEE by nanopillars is expectable if proper optimizations discussed above can be achieved: a thinner membrane, longer nanopillars, an optimized diameter and pitch distance. Furthermore, it is of great interest to explore *sub-threshold field emission* from nanopillars, i.e., an even higher electrical field together with bombardment from incident electrons helps to increase the emission probability [15, 16]. A higher yield of SEE can

[3] Different to the conventional definition of secondary electron yield, here the yield γ_p and γ_m include both the transmitted electrons and the true secondary electrons.

also be realized by choosing materials with higher intrinsic yield of SEE, e.g., diamond [17]. Here, we emphasize that integration of nanopillars on a membrane has two obvious advantages: (i) they naturally provide a boost to SEE by the geometrical change of the emission surface, as we have seen, and (ii) they constitute an array of pointing emitters operating *in parallel*, which has great potential for including other emission mechanisms such as electron field emission and plasmon/phonon/photon-assisted tunneling.

4. Summary

In summary we have demonstrated that an NPM system can be engineered and optimized to maximize the SEY. Electron–solid interactions in the world of nanoobjects will demonstrate new effects and find applications in new-concept devices. Particularly in the device shown here, the functions of the membrane and nanopillars are separated in a sense that the membrane acts as a filter/window for incident particles, while the nanopillars are the true active elements. It is clear that the geometry of the nanopillars and the arrays can be freely chosen. One can use a host of different heterostructure materials, such as p–n junctions and quantum wells, to integrate into the NPM system, which enhances the functionality. Finally, the nanopillars can be further configured as electron field emitters, where they serve not only as a host of particle–solid interaction, but also as probes of electronic/mechanical excitations in NPM systems disturbed by incident particles or radiation.

Acknowledgments

The authors thank Michael S Westphall and Lloyd M Smith for helpful discussions and comments. The authors would like to acknowledge support from the Wisconsin Alumni Research Foundation (WARF), the National Science Foundation (MRSEC-IRG1), and the Air Force RSO under contract number F49620-03-1-0420.

References

[1] Bruining H 1954 *Physics and Applications of Secondary Electron Emission* (New York: McGraw-Hill)
[2] Wilcock W L, Emberson D L and Weekley B 1960 *Nature* **185** 370
[3] Johnson J B and McKay K G 1954 *Phys. Rev.* **93** 668
[4] Kanter H 1961 *Phys. Rev.* **121** 677
[5] Egerton R F 1986 *Electron Energy-Loss Spectroscopy in the Electron Microscope* (New York: Plenum)
[6] Stab L 1990 *Nucl. Instrum. Methods* A **288** 24
[7] Kamiya T, Cholewa M, Saint A, Prawer S, Legge G J F, Butler J E and Vestyck D J Jr 1997 *Appl. Phys. Lett.* **71** 1875
[8] Porter F S, McCammon D, Galeazzi M and Stahle C K (eds) 2001 *Low Temperature Detectors: 9th Int. Workshop on Low Temperature Detectors*; *AIP Conf. Proc.* **605** 1
[9] Nishimura K, Itotani T and Ohya K 1994 *Japan. J. Appl. Phys.* **33** 4727
[10] Suzuki M, Yamada T and Yang C Y 2007 *Appl. Phys. Lett.* **90** 083111
[11] Crewe A V, Wall J and Langmore J L 1970 *Science* **168** 1338
[12] Browning N D, Chisholm M F and Pennycook S J 1993 *Nature* **366** 143
[13] Bethe A 1933 *Handbuch der Physik* vol 24 (Berlin: Springer)
[14] Joy D C 1995 *Monte Carlo Modeling for Electron Microscopy and Microanalysis* (New York: Oxford University Press)
[15] Nojeh A, Shan B, Cho K and Pease R F W 2006 *Phys. Rev. Lett.* **96** 056802
[16] Qin H, Kim H S, Westphall M S, Lloyd L M and Blick R H 2007 Subthreshold field emission from thin silicon membranes *Appl. Phys. Lett.* **91** 183506
[17] Geis M W, Efremov N N, Krohn K E, Twichell J C, Lyszczarz T M, Kalish R, Greer J A and Tabat M D 1998 *Nature* **393** 431